Available online at www.sciencedirect.com
ScienceDirect
Journal of Sound and Vibration 317 (2008) 91–111
JOURNAL OF SOUND AND VIBRATION
www.elsevier.com/locate/jsvi

A finite element model for sandwich viscoelastic beams: Experimental and numerical assessment

F.S. Barbosa*, M.C.R. Farage

Federal University of Juiz de Fora, Faculty of Engineering, Graduation Program in Computational Modelling, Campus Universitário de Martelos, CEP 36036-330, Juiz de Fora, MG, Brazil

Received 16 April 2007; received in revised form 28 February 2008; accepted 3 March 2008
Handling Editor: S. Bolton
Available online 9 May 2008

Abstract

Among the passive control systems for attenuation of vibrations in structures, those that use viscoelastic materials as a damping core in laminated-plate-like components are focused herein. In the present work an assessment of a time-domain formulation for numerical modelling of viscoelastic materials is made. This formulation, which is called Golla–Hughes method (GHM), is based on a second-order time-domain realization of Laplace-domain motion equations. The GHM parameters used in the characterization of a viscoelastic material are experimentally determined and a sandwich GHM-based finite element model is presented and validated through numerical comparisons with classic formulation results. Finally, a time-domain simulation of an experimentally tested sandwich beam is carried out.

1. Introduction

The modelling of viscoelastic materials has two main applications. Firstly, the simulation of rheological problems, which is known as quasi-static analysis due to the fact that the inertial forces involved in the problem are not taken into account. The classic models of Maxwell, Voigt and Kelvin and Refs. [1,2] are typical examples of such models. Secondly, real dynamic problems involving viscoelastic materials have also been studied since the 1950s in the works of Oberst and Frankenfeld [3], Kervin [4] and Ross et al. [5]. In general, these kind of models simulate the dynamic structural behavior of the viscoelastic material working as passive vibration control systems.

Vibration control systems assembled to structures, like the sandwich viscoelastic systems, have experienced a growth in practical applications due to some benefits related to cost-effectiveness and a high level of dynamic damping [6–9]. One of the first large-scale practical applications of sandwich viscoelastic elements in order to reduce vibrations was the World Trade Center, New York, USA. Some features of this kind of project were studied by Mahmoodi [10] and Samali and Kwok [11]. In Brazil, Battista et al. [8] developed dynamic tests in a 1:1 scale prototype of Rio–Niterói bridge (Rio de Janeiro, Brazil) central spam. This work consisted of a very

*Corresponding author. Tel.: +55 32 2102 3424; fax: +55 32 2102 3401.
E-mail addresses: flavio.barbosa@ufjf.edu.br (F.S. Barbosa), michele.farage@ufjf.edu.br (M.C.R. Farage).

0022-460X/$ - see front matter © 2008 Elsevier Ltd. All rights reserved.
doi:10.1016/j.jsv.2008.03.013

comprehensive experimental program, including comparisons between the dynamic behavior of a concrete/steel deck and a sandwich (concrete/viscoelastic material/steel) deck, leading to the conclusion that the sandwich deck has damping ratio considerably superior for high frequencies in this kind of application.

In order to model those systems, it is necessary a formulation which takes into account the temperature and frequency dependence of the Young's modulus and damping properties of the viscoelastic material. When the relevant response of a sandwich viscoelastic system is framed in a short time interval, or when the analysis can be done piecewisely, the temperature dependence may be ignored [8,10]. The consideration of frequency-dependent viscoelastic properties is usually made in the frequency-domain. Clough and Penzien [12] affirm that "when the equation of motion contains parameters which might be frequency dependent, such as stiffness or damping, the frequency-domain approach is much superior to the time-domain approach".

Despite this previous statement, time-domain approaches are also employed to modelling viscoelastic materials or composite structures in an efficient manner. These approaches are generally developed in the framework of finite element method (FEM). Qian and Demao [13] made an attempt to build a theory analysis and a series of numerical methods for dynamic behavior of sandwich structures, by using virtual work principles and deriving finite element method in time-domain. Kaliske and Rothert [14] present a linear viscoelastic finite element approach which was used to modelling rubbers and more specifically tires. A finite element sandwich model for harmonically excited viscoelastic sandwich beams is proposed by Babert, Maddox and Orozco [15]. Zapfe and Lesieutre [16] propose a discrete layer finite element for dynamic analysis of laminated beams which appears to be efficient in the transverse shear treatment in the analysis of sandwich structures. The finite element method presented by Yi et al. [17] is interesting since it considers a viscoelastic damping layer working together with a smart piezoelectric constrained layer. Golla and Hughes [18] present a time-domain formulation to modelling viscoelastic materials based on a second-order time-domain realization of Laplace-domain motion equations which yields a linear differential formulation that includes an augment in the set of generalized coordinates.

In the present work, a numerical–experimental assessment of the Golla–Hughes Method (GHM) [18] time-domain formulation for numerical modelling of viscoelastic materials is carried out. A GHM-based sandwich Finite Element model is proposed and the parameters which characterize the viscoelastic material are experimentally determined. The theoretical formulation and the implemented solution method are thoroughly assessed by means of comparisons between numerical results and their experimental counterpart, demonstrating the favorable performance of this mathematical–numerical model.

2. The formulation of Golla–Hughes method

This section summarizes the Golla–Hughes method detailed in Ref. [18].

The complex Young's modulus ($\mathscr{E}(s)$) may be expressed in Laplace-domain as

$$\mathscr{E}(s) = \varepsilon + h(s), \tag{1}$$

where ε is the elastic part of the complex modulus, $h(s)$ is the dissipation function associated to the damping and s is the Laplace variable. Biot [19] proposed a dissipation function as shown in Eq. (2)[1].

$$h(s) = \sum_{i=1}^{n} \frac{a_i s}{s + b_i}, \tag{2}$$

where a_i and b_i are obtained from curve-fitting experimental curves.

As the complexity of GHM models is directly associated to the number of dissipation function terms, it was adopted a two terms approach for the Biot's dissipation function, resulting in

$$h(s) = \frac{\alpha(s^2 + \beta s)}{s^2 + \beta s + \delta}, \tag{3}$$

where $\alpha = a_1 + a_2$, $\gamma = a_1 b_2 + a_2 b_1$, $\beta = b_1 + b_2$ and $\delta = b_1 b_2$.

[1]Bagley and Torvik [20] proposed a fractional derivative model for dissipation functions which shows good agreement with experimental results.

The dynamic equilibrium equation for a single-degree-of-freedom (dof) system in Laplace-domain, considering null initial conditions and Eq. (1), may be written as

$$[s^2\mathscr{M} + \mathscr{E}(s)\mathscr{K}]q(s) = [s^2\mathscr{M} + \varepsilon\mathscr{K} + h(s)\mathscr{K}]q(s) = f(s), \tag{4}$$

where $\mathscr{M}$ is the mass of the system; $\mathscr{K}$ is part of the system stiffness which excludes the complex modulus expressed in Laplace-domain; $q(s)$ is the degree-of-freedom and $f(s)$ is the excitation.

The aim of GHM is to express Eq. (4) in the time-domain using a particular inverse Laplace transformation[2], which consists in a second order time-domain realization of Laplace-domain motion equation. It can be noticed that all the terms of Eq. (4) have a simple inverse Laplace transformation except the term $h(s)q(s)$, which includes a product of two functions of s. GHM admits that $\mathscr{H} = \mathscr{L}^{-1}[h(s)q(s)]$ exists and it can be expressed as

$$\begin{bmatrix} M & m \\ m & 1 \end{bmatrix} \begin{Bmatrix} \ddot{q}(t) \\ \ddot{z}(t) \end{Bmatrix} + \beta \begin{bmatrix} D & d \\ d & 1 \end{bmatrix} \begin{Bmatrix} \dot{q}(t) \\ \dot{z}(t) \end{Bmatrix} + \delta \begin{bmatrix} K & k \\ k & 1 \end{bmatrix} \begin{Bmatrix} q(t) \\ z(t) \end{Bmatrix} = \begin{Bmatrix} \mathscr{H} \\ 0 \end{Bmatrix}, \tag{5}$$

where M, D, K, m, d and k are unknowns; z is an additional degree-of-freedom and t is the time variable.

In order to validate this assumption, the first line of the matrix Eq. (5) must represent $\mathscr{L}^{-1}[h(s)q(s)] = \mathscr{H}$ and the second line must present an identity.

By expanding the matrix Eq. (5), the following equations are obtained:

$$M\ddot{q}(t) + m\ddot{z}(t) + \beta D\dot{q}(t) + \beta d\dot{z}(t) + \delta Kq(t) + \delta kz(t) = \mathscr{H}, \tag{6}$$

$$m\ddot{q}(t) + \ddot{z}(t) + \beta d\dot{q}(t) + \beta\dot{z}(t) + \delta kq(t) + \delta z(t) = 0. \tag{7}$$

The Laplace transformations of Eqs. (6) and (7) are expressed in the following equations, respectively:

$$Mq(s)s^2 + mz(s)s^2 + \beta Dq(s)s + \beta dz(s)s + \delta Kq(s) + \delta kz(s) = h(s)q(s), \tag{8}$$

$$mq(s)s^2 + z(s)s^2 + \beta dq(s)s + \beta z(s)s + \delta kq(s) + \delta z(s) = 0. \tag{9}$$

Regrouping the terms in $q(s)$ and $z(s)$ from Eqs. (8) and (9) leads to the following equations, respectively:

$$(Ms^2 + \beta Ds + \delta K)q(s) + (ms^2 + \beta ds + \delta k)z(s) = h(s)q(s). \tag{10}$$

$$(ms^2 + \beta ds + \delta k)q(s) + (s^2 + \beta s + \delta)z(s) = 0. \tag{11}$$

Replacing $z(s)$ in Eq. (10) for its expression obtained from Eq. (11) and considering $h(s)$ from Eq. (3) leads to

$$(Ms^2 + \beta Ds + \delta K) - \frac{(ms^2 + \beta ds + \delta k)^2}{s^2 + \beta s + \delta} = \frac{\alpha s^2 + \gamma s}{s^2 + \beta s + \delta}. \tag{12}$$

Regrouping the coefficients of s and after some mathematical manipulations, Eq. (12) can be rewritten in the form:

$$\begin{aligned}(M - m^2)s^4 + (M\beta + D\beta - 2md\beta)s^3 + (M\delta + D\beta^2 + K\delta - d^2\beta - 2mk\delta - \alpha)s^2 \\ + (D\beta\delta + K\beta\delta - 2dk\beta\delta - \gamma)s + (K\delta^2 - k\delta^2) = 0.\end{aligned} \tag{13}$$

In order to satisfy Eq. (13) each coefficient of s has to be equal to zero, resulting in the five following algebraic equations:

$$M - m^2 = 0, \tag{14}$$

$$M + D - 2md = 0 \quad (\beta \neq 0), \tag{15}$$

$$M\delta + D\beta^2 + K\delta - d^2\beta^2 - 2mk\delta = \alpha, \tag{16}$$

[2]Barrett and Gotts [21] also deals with Laplace-domain in order to simulate the dynamic behavior of viscoelastic systems.

$$D + K - 2dk = \gamma/(\beta\delta), \quad (\beta\delta \neq 0), \tag{17}$$

$$K - k^2 = 0. \tag{18}$$

There are infinite solutions for this system of algebraic equations. The chosen solution considers the restriction $\gamma = \alpha\beta$, leading to

$$D = 0, \tag{19}$$

$$M = 0, \tag{20}$$

$$K = \alpha/\delta, \tag{21}$$

$$d = 0, \tag{22}$$

$$m = 0, \tag{23}$$

$$k = \sqrt{\alpha/\delta}. \tag{24}$$

Obviously, the adopted restriction is only valid if the experimental curves of the considered viscoelastic material allow this kind of simplification. Replacing the chosen solution in Eq. (5) and omitting the time variable t leads to the following:

$$\begin{bmatrix} 0 & 0 \\ 0 & 1 \end{bmatrix} \begin{Bmatrix} \ddot{q} \\ \ddot{z} \end{Bmatrix} + \beta \begin{bmatrix} 0 & 0 \\ 0 & 1 \end{bmatrix} \begin{Bmatrix} \dot{q} \\ \dot{z} \end{Bmatrix} + \delta \begin{bmatrix} \alpha/\delta & \sqrt{(\alpha/\delta)} \\ \sqrt{(\alpha/\delta)} & 1 \end{bmatrix} \begin{Bmatrix} q \\ z \end{Bmatrix} = \begin{Bmatrix} \mathscr{H} \\ 0 \end{Bmatrix}. \tag{25}$$

Eq. (25) may be rewritten in a simpler form, by changing the variables $y = z\sqrt{\delta/\alpha}$ producing the following equation where y is known as the dissipation variable:

$$\alpha/\delta \begin{bmatrix} 0 & 0 \\ 0 & 1 \end{bmatrix} \begin{Bmatrix} \ddot{q} \\ \ddot{y} \end{Bmatrix} + \frac{\alpha\beta}{\delta} \begin{bmatrix} 0 & 0 \\ 0 & 1 \end{bmatrix} \begin{Bmatrix} \dot{q} \\ \dot{y} \end{Bmatrix} + \alpha \begin{bmatrix} 1 & 1 \\ 1 & 1 \end{bmatrix} \begin{Bmatrix} q \\ y \end{Bmatrix} = \begin{Bmatrix} \mathscr{H} \\ 0 \end{Bmatrix}. \tag{26}$$

By using $\mathscr{H}$ value from Eq. (26), the particular inverse Laplace transformation of a single degree-of-freedom system constituted by viscoelastic material, Eq. (5), may be expressed in the following form:

$$\begin{bmatrix} \mathscr{M} & 0 \\ 0 & \alpha/\delta\mathscr{K} \end{bmatrix} \begin{Bmatrix} \ddot{q}(t) \\ \ddot{y}(t) \end{Bmatrix} + \begin{bmatrix} 0 & 0 \\ 0 & \alpha\beta/\delta\mathscr{K} \end{bmatrix} \begin{Bmatrix} \dot{q}(t) \\ \dot{y}(t) \end{Bmatrix} + \begin{bmatrix} (\varepsilon+\alpha)\mathscr{K} & \alpha\mathscr{K} \\ \alpha\mathscr{K} & \alpha\mathscr{K} \end{bmatrix} \begin{Bmatrix} q(t) \\ y(t) \end{Bmatrix} = \begin{Bmatrix} f(t) \\ 0 \end{Bmatrix}. \tag{27}$$

Despite the lack of physical meaning of the dissipation variable $y(t)$, it is possible to describe its mechanical interpretation as shown in Fig. 1. This figure presents the well-known Maxwell model with a linear spring connected in parallel forming a linear standard model, inducing that this GHM-based model is, in fact, a different way to interpret it.

By using an analog process and some additional considerations described in Ref. [18], it is possible to achieve the system of differential equations for a multi-degree-of-freedom finite element model as

$$\mathbf{M}^v \begin{Bmatrix} \ddot{\mathbf{q}}(t) \\ \ddot{\mathbf{y}}(t) \end{Bmatrix} + \mathbf{C}^v \begin{Bmatrix} \dot{\mathbf{q}}(t) \\ \dot{\mathbf{y}}(t) \end{Bmatrix} + \mathbf{K}^v \begin{Bmatrix} \mathbf{q}(t) \\ \mathbf{y}(t) \end{Bmatrix} = \begin{Bmatrix} \mathbf{f}(t) \\ \mathbf{0} \end{Bmatrix}, \tag{28}$$

where

$$\mathbf{M}^v = \begin{bmatrix} \mathbf{M}^e & \mathbf{0} \\ \mathbf{0} & \alpha/\delta\mathbf{I} \end{bmatrix}, \tag{29}$$

$$\mathbf{C}^v = \begin{bmatrix} \mathbf{0} & \mathbf{0} \\ \mathbf{0} & \alpha\beta/\delta\mathbf{I} \end{bmatrix}, \quad \text{and} \tag{30}$$

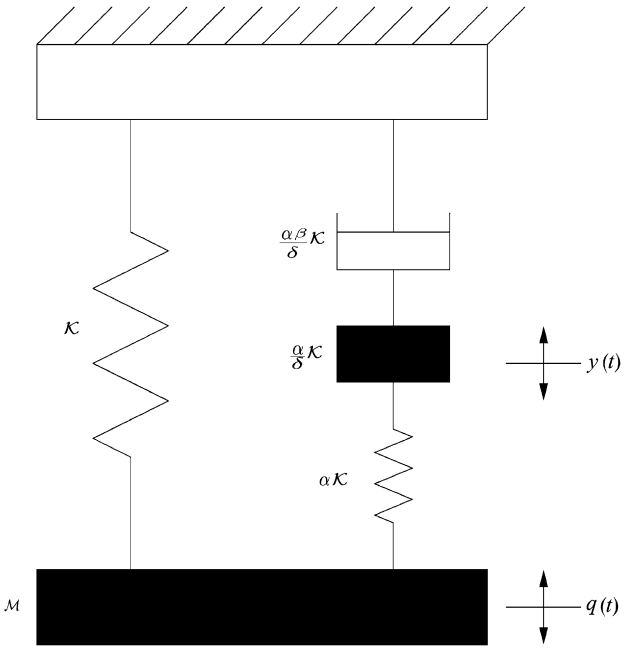

Fig. 1. Mechanical interpretation of the adopted Golla–Hughes method model.

$$\mathbf{K}^v = \begin{bmatrix} (\varepsilon + \alpha)\mathbf{K}^e & \alpha\mathbf{R} \\ \alpha\mathbf{R}^T & \alpha\mathbf{I} \end{bmatrix} \tag{31}$$

are, respectively, the mass, damping and stiffness matrices of the viscoelastic finite element (^{v} denotes viscoelastic matrices); where $\mathbf{M}^e$ is the finite element mass matrix considering an elastic system; $\mathbf{K}^e$ is the finite element stiffness matrix considering an elastic system and excluding the Young's modulus (^{e} denotes elastic matrices); $\mathbf{q}(t)$, $\dot{\mathbf{q}}(t)$ and $\ddot{\mathbf{q}}(t)$ are, respectively, the displacement, velocity and acceleration vectors of the real degrees-of-freedom; $\mathbf{y}(t)$, $\dot{\mathbf{y}}(t)$ and $\ddot{\mathbf{y}}(t)$ are, respectively, the displacement, velocity and acceleration vectors of the dissipation degrees-of-freedom; $\mathbf{0}$ and $\mathbf{I}$ represents, respectively, the null and the identity matrix or vector; $\mathbf{f}(t)$ is the force vector; $\mathbf{R} = \mathbf{R}_d\boldsymbol{\Lambda}_d^{1/2}$; $\mathbf{R}_d$ is the matrix whose columns are the eigenvectors of $\mathbf{K}^e$ associated to the non-rigid body modes; and $\boldsymbol{\Lambda}_d$ is the diagonal matrix with the related eigenvalues of $\mathbf{R}_d$.

The dimension of the viscoelastic matrices depends on the dimension of the related elastic finite element and the amount of dissipation variables. Each physical degree-of-freedom implies one dissipation variable, although it is necessary to exclude those associated to rigid modes of $\mathbf{K}^e$. For example, for a four nodes plane quadrilateral linear finite element with two degrees-of-freedom (vertical and horizontal displacements) per node, there are eight real degrees-of-freedom and five dissipation variables: 8 real degrees-of-freedom–3 rigid modes (two translations and one rotation) $=$ 5. In this case the dimension of the viscoelastic matrices is $8 + 5 = 13$.

Finally, GHM parameters obtained from experimental data (ε, α, β and δ) and Eqs. (29)–(31) allow the determination of the viscoelastic finite element matrices for any kind of finite element model.

3. Determination of GHM parameters from experimental data

Eq. (1) may also be expressed in the frequency-domain, considering the dissipation function of Eq. (3):

$$E^*(\omega) = \varepsilon + \frac{\alpha(-\omega^2 + \mathrm{i}\beta\omega)}{-\omega^2 + \mathrm{i}\beta\omega + \delta}, \tag{32}$$

where $E^*(\omega)$ is the complex modulus expressed in the frequency-domain; $\mathrm{i} = \sqrt{-1}$; and ω is the frequency variable.

Commonly this complex modulus is divided into two parts: E' is the real part, known as storage modulus; and η is the ratio between the imaginary and real parts, E''/E' are known as loss factor.

Eqs. (33) and (34) express, respectively, E' and η:

$$E' = \varepsilon + \frac{\alpha\omega^2(\omega^2 - \delta + \beta^2)}{(\delta - \omega^2)^2 + \beta^2\omega^2}, \tag{33}$$

$$\eta = \frac{\alpha\beta\omega\delta}{(\delta - \omega^2)^2 + \beta^2\omega^2}\frac{1}{E'}. \tag{34}$$

The parameters ε, α, β, δ in Eqs. (33) and (34) are in general obtained from curve fitting experimental results given in terms of $E'(\omega)$ and $\eta'(\omega)$. In this work, experimental tests based on "ASTM Standard Test Method for Measuring Vibration-Damping Properties of Materials" [22] were developed in order to determine these parameters.

The experimental program concerned 6 beams of different lengths divided in two groups: a set of three simple beams, presented in Fig. 2 and a set of three sandwich beams, presented in Fig. 3. The simple set is composed by three elastic clumped–free aluminum beams having one single layer, and the sandwich set has three viscoelastic sandwich clumped–free beams, having two layers of aluminum and the viscoelastic material in the core composed by a Scott double-face adhesive 3M Scotch© double adherent faces. For each set, it was tested three specimens lengths (L): 0.50, 0.80 and 1.00 m. A photo of a typical tested sample and the beam test scheme are presented in Figs. 4 and 5, respectively, showing the excited and the observed points valid for both sets.

The dynamic responses of the beams were obtained by means of accelerometer's measurements during a free vibration tests performed by employing instantaneous hammer impact as excitation. Figs. 6(a)–(c) present typical time responses in terms of vertical accelerations for 0.50, 0.80 and 1.00 m long beams, respectively.

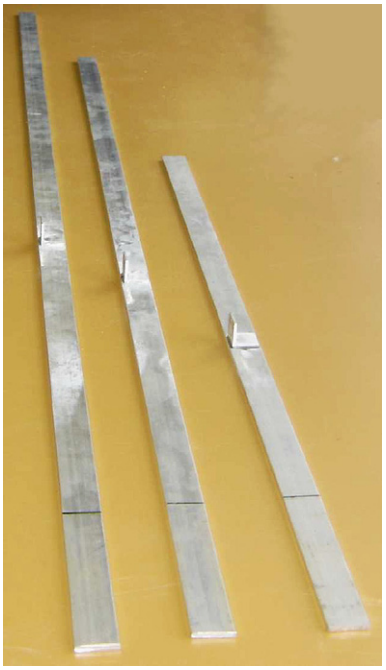

Fig. 2. Picture of the simple set.

Fig. 3. Picture of the sandwich set.

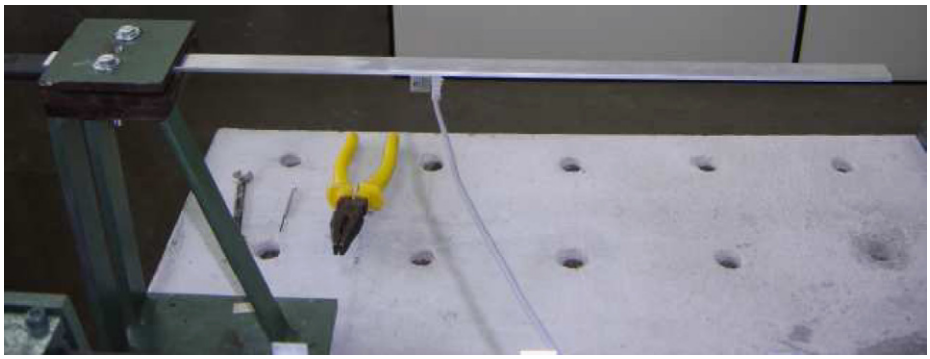

Fig. 4. Picture of a typical specimen test setup.

The main features of the used equipment and the data acquisition are: accelerometer model AS-GA Kyowa [23], rated capacity ±2 g (safe overloading 300%); acquisition system: Lynx ADS2000 [24]; frequency of acquisition 1000 Hz; low-pass filtering via hardware in 200 Hz; and time of acquisition: 1 s.

ASTM [22] recommends the use of non-contacting-type transducers for the dynamic test measurements. As this kind of equipment is not available in the test laboratory, the accerelometers weight influence in the dynamic behavior of the tested beams demands additional analysis.

The experimental results in terms of the tree first natural frequencies, loss factor and respective standard deviations for the simple and the sandwich sets are presented in Tables 1 and 2, respectively. The modal identification was carried out using random decrement method [25] and Ibrahim time-domain method [26]. Each sample was subjected to 4 tests and modal identifications were carried out about 200 times, taking different parts of the responses. Table 1 also presents theoretical natural frequencies for the simple set obtained with

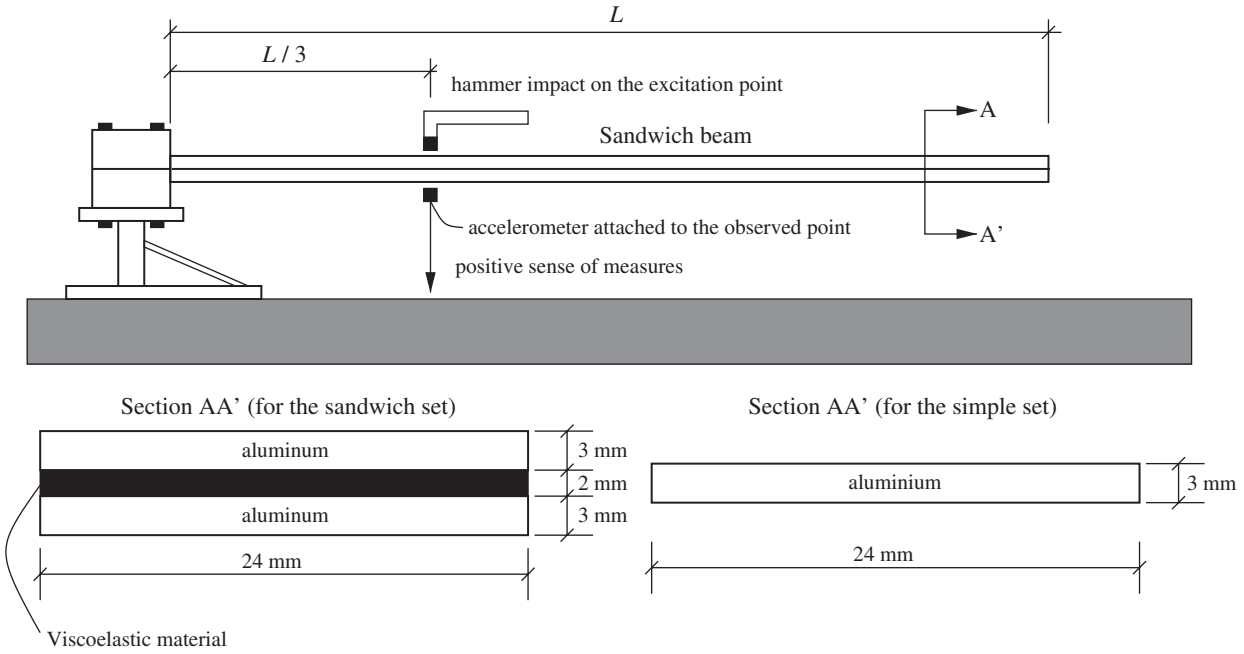

Fig. 5. Typical schema of the tests.

$$f_n = r_n \sqrt{\frac{EI}{\bar{m}L^4}}, \tag{35}$$

where f_n, $(n = 1 \ldots 3)$, are the natural undamped frequencies of the system (in Hz); $E = 68.7\,\text{GPa}$ is the adopted aluminum Young's modulus; $I = 5.40 \times 10^{-11}\,\text{m}^4$ is the cross-section moment of inertia; $\bar{m} = 0.1937\,\text{kg/m}$ is the mass per unit of length; and $\mathbf{r} = \{0.560, 3.507, 9.820\}$.

By observing percentage differences between the theoretical and experimental results shown in Table 1, it is noticed that the influence of accelerometer weight is more significant for the dynamic behavior of 0.50 m long beam. These results reduce test reliabilities, but they are not significant enough in order to invalidate them.

Except for the third natural frequency of the 0.50 m long simple sample, all the identified natural frequencies have standard deviation lower than 4%. The major part of natural frequencies had standard deviation inferior to 1%. In terms of damping identification, the standard deviations were more significant, in accordance with damping results presented in Ref. [27], and the mean values are not very different from those obtained by Faisca [28].

By applying Eqs. (36)–(39) (retyped from Ref. [22]) with the results of mean natural frequencies and mean loss factor obtained from the two tested sets, presented in Tables 1 and 2, it is possible to calculate E' and η for the viscoelastic material in the discrete values of natural frequencies of the sandwich set.

$$E_{2n} = 2(1+\nu)\frac{(A-B) - 2(A-B)^2 - 2(A\eta_n)^2}{(1-2A+2B)^2 + 4(A\eta_n)^2}\frac{E_1 H_1 H_2 a_n}{L^2}, \tag{36}$$

$$\eta_{2n} = \frac{A\eta_n}{(A-B) - 2(A-B)^2 - 2(A\eta_n)^2}, \tag{37}$$

$$A = \left(\frac{\omega_n}{\omega_{1n}}\right)^2 (2 + \rho_r h_2)\left(\frac{B}{2}\right), \tag{38}$$

$$B = \frac{1}{6(1+h_2)^2}, \tag{39}$$

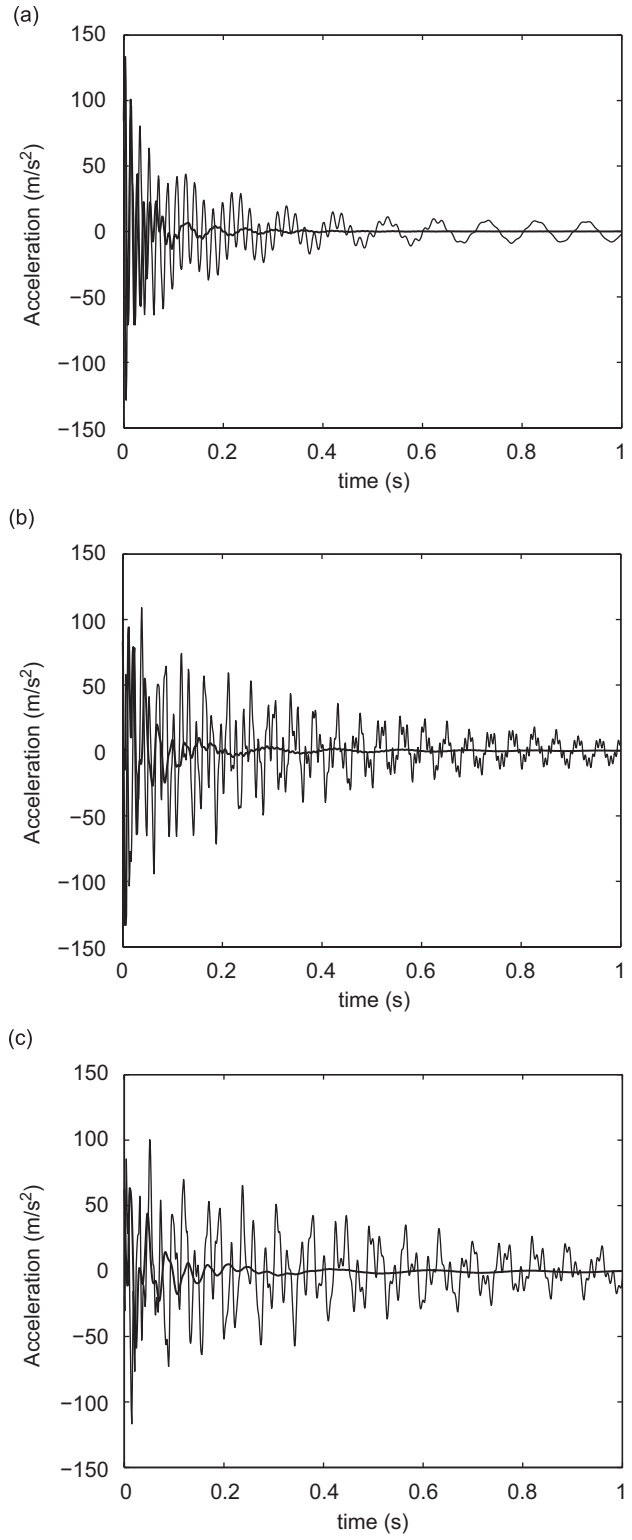

Fig. 6. Typical time series for simple (thin lines) and sandwich (thick lines) specimens: (a) $L = 0.5\,\mathrm{m}$; (b) $L = 0.8\,\mathrm{m}$ and (c) $L = 1.0\,\mathrm{m}$.

Table 1
Summary of experimental results for the simple set and the respective theoretical natural frequencies

	$L = 1.00\,\text{m}$	$L = 0.80\,\text{m}$	$L = 0.50\,\text{m}$
f_1^{exp}	2.67 ± 0.10	3.99 ± 0.05	9.98 ± 0.01
f_1^{the}	2.45	3.83	9.80
$(f_1^{\text{teo}} - f_1^{\text{exp}})/f_1^{\text{exp}}$	-8.24%	-4.51%	-1.80%
η_1	0.0960 ± 0.0512	0.0244 ± 0.0298	0.0104 ± 0.0020
f_2^{exp}	15.44 ± 0.03	22.77 ± 0.04	54.28 ± 0.09
f_2^{the}	15.35	23.98	61.39
$(f_2^{\text{teo}} - f_2^{\text{exp}})/f_2^{\text{exp}}$	-0.58%	5.31%	13.10%
η_2	0.0256 ± 0.0028	0.0250 ± 0.0180	0.0380 ± 0.0066
f_3^{exp}	42.93 ± 0.08	63.62 ± 0.09	157.72 ± 11.85
f_3^{the}	42.96	67.15	171.90
$(f_3^{\text{teo}} - f_3^{\text{exp}})/f_3^{\text{exp}}$	0.07%	5.55%	8.99%
η_3	0.0210 ± 0.0206	0.0258 ± 0.0180	0.0730 ± 0.0356

($^{\text{exp}}$) denotes mean experimental values; ($^{\text{the}}$) denotes theoretical values; and ($_n$) denotes the nth natural frequency or loss factor ($n = 1 \ldots 3$). Frequencies are presented in Hz.

Table 2
Summary of experimental results for the sandwich set

	$L = 1.00\,\text{m}$	$L = 0.80\,\text{m}$	$L = 0.50\,\text{m}$
f_1	5.05 ± 0.02	7.55 ± 0.03	16.95 ± 0.04
η_1	0.1434 ± 0.0084	0.1770 ± 0.0062	0.1748 ± 0.0060
f_2	24.54 ± 0.69	37.13 ± 0.08	79.33 ± 0.16
η_2	0.1508 ± 0.0374	0.1768 ± 0.0058	0.0765 ± 0.0102
f_3	60.13 ± 0.31	93.18 ± 2.41	184.44 ± 3.00
η_3	0.1754 ± 0.0098	0.0788 ± 0.0668	0.1350 ± 0.0142

($_n$) denotes the nth natural frequency or loss factor ($n = 1 \ldots 3$). Frequencies are presented in Hz.

where h_2 is the ratio between the viscoelastic core thickness and the elastic layer thickness ($h_2 = H_2/H_1$); ω_n and η_n are the nth natural frequency and loss factor of the sandwich beam set; ω_{1n} is the the nth natural frequency of the simple set; ρ_r is the ratio between viscoelastic and elastic material densities; L is the beam length; E_{2n} and $v = 0.25$ are, respectively, the Young's modulus and the Poisson ratio of the viscoelastic material; and $\mathbf{a} = \{3.516, 22.035, 61.697\}$.

Discrete points in Figs. 7 and 8 are, respectively, the storage modulus E' and the loss factor η of the tested viscoelastic material and the plotted solid lines are Eqs. (33) and (34) obtained by curve-fitting viscoelastic parameters α, β, δ and ε. The curve fit procedure was carried out using least-squares method and the discrete experimental points of E' and η, resulting in: $\alpha = 5.26\,\text{MPa}$, $\beta = 55.59 \times 10^6\,\text{s}^{-1}$, $\delta = 6.98 \times 10^9\,\text{s}^{-2}$ and $\varepsilon = 0.58\,\text{MPa}$. The quality of the curve fitting is limited by the amount of parameters adopted in the GHM model. The fitted curves may be improved by means of a Biot's representation (see Eq. (2)) based on more than two terms, which leads to a GHM model with more than four parameters and results in a completely different finite element model, rather more complex than the one dealt herein.

4. The sandwich viscoelastic model

The proposed sandwich viscoelastic model is presented in Fig. 9. It is composed by a combination of seven finite elements: two elastic frame elements (with two nodes each one); one quadrilateral linear viscoelastic

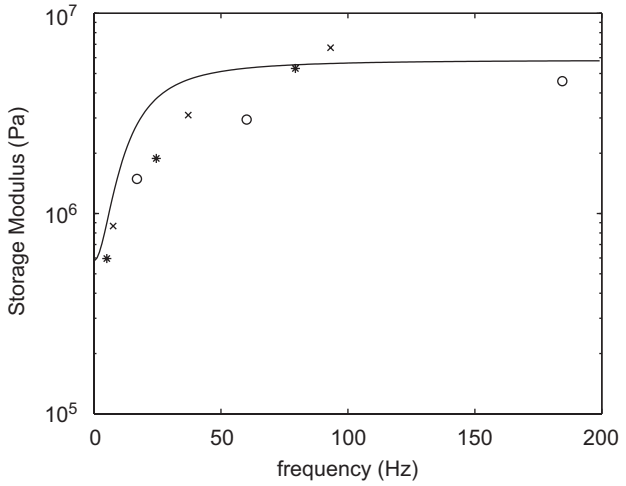

Fig. 7. Experimental results and the fitted curve for storage modulus of the tested viscoelastic material. Solid line: fitted curve; (o) experimental results for 0.50 m long beam; (×) experimental results for 0.80 m long beam; (*) experimental results for 1.00 m long beam.

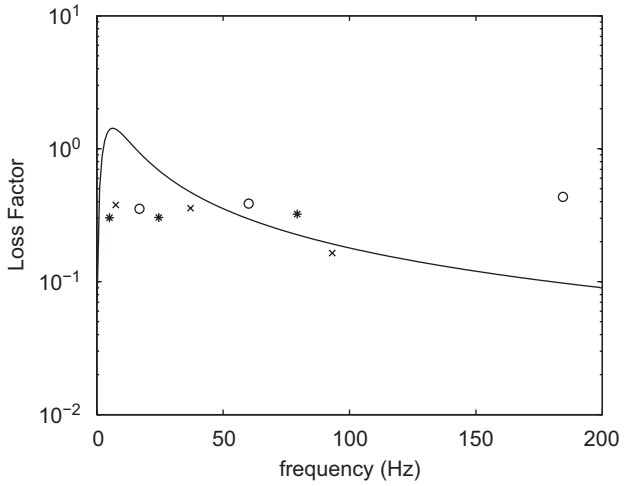

Fig. 8. Experimental results and the fitted curve for loss factor of the tested viscoelastic material. Solid line: fitted curve; (o) experimental results for 0.50 m long beam; (×) experimental results for 0.80 m long beam; (*) experimental results for 1.00 m long beam.

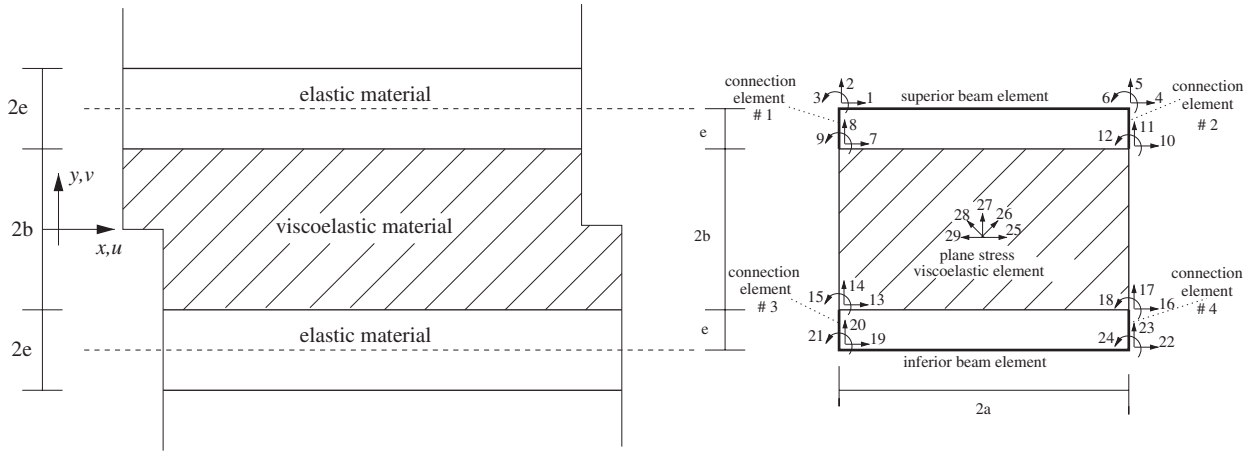

Fig. 9. Sandwich finite element model composed by the assembly of seven finite element.

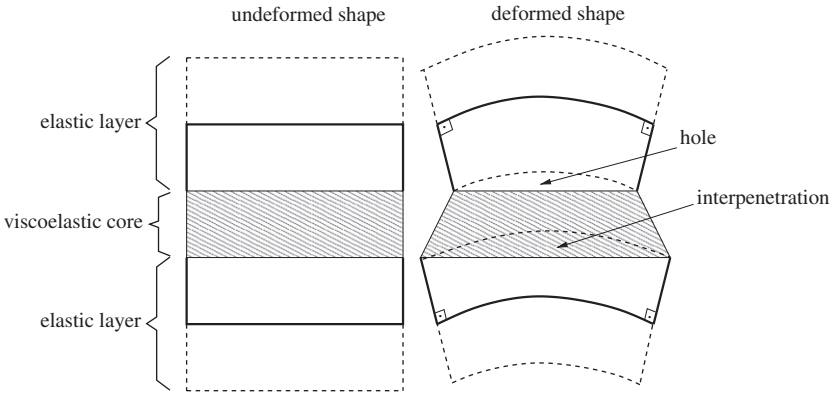

Fig. 10. Undeformed and deformed shape of the proposed finite element model.

plate element (with four nodes); and four rigid connection elements (with two nodes each one). The model has 24 physical degrees-of-freedom (q_1 to q_{24}, numbered from 1 to 24), and 5 dissipation variables (y_1 to y_5, numbered from 25 to 29), resulting in a super element model matrix dimension of 29. The dissipation variable directions plotted in Fig. 9 have no physical interpretation.

The kinematics assumptions of the proposed finite element model assure deflection deformations in the viscoelastic core as shown in Fig. 10, introducing shearing effects. It is possible to observe that the proposed sandwich finite element model allows discontinuity in the displacement field between the frames and the quadrilateral viscoelastic linear element. In this case, errors inherent to the proposed finite element model must be investigated through the mesh convergence analysis.

Another limitation of the model concerns the core thickness. Thick cores introduce high-order vibration modes, leading each elastic layer of the sandwich beam to vibrate isolated.

In order to compute the contribution of each kind of finite element in the composition of the sandwich finite element model matrices, the problem is decomposed in three parts: contribution of the two elastic beam elements; contribution of the rectangular viscoelastic element; and contribution of the four connection elements.

4.1. Contribution of the two elastic frame elements

For the sake of simplicity, the following is adopted: Being a n-dimensional square matrix $\mathbf{H}$; a k and a p-dimensional vectors $\mathbf{l}$ and $\mathbf{c}$, respectively, being $1 \leqslant k, p \leqslant n$, $\mathbf{H}_{\mathbf{l},\mathbf{c}}$ is defined as a sub-matrix of $\mathbf{H}$ having $\mathbf{l}$ lines and $\mathbf{c}$ columns.

Being $\mathbf{M}$, $\mathbf{K}$ and $\mathbf{C}$ the super element model matrices, the individual matrix contributions of each beam for the finite element model of Fig. 9 is well known and presented in Eqs. (40)–(42), representing the mass, damping and stiffness matrix contributions, respectively

$$\mathbf{M}_{\mathbf{l},\mathbf{c}} = \begin{bmatrix} 140m & 0 & 0 & 70m & 0 & 0 \\ 0 & 156m & 22mL & 0 & 54m & -13mL \\ 0 & 22mL & 4mL^2 & 0 & 13mL & -3mL^2 \\ 70m & 0 & 0 & 140m & 0 & 0 \\ 0 & 54m & 13mL & 0 & 156m & -22mL \\ 0 & -13mL & -3mL^2 & 0 & -22mL & 4mL^2 \end{bmatrix}, \tag{40}$$

$$\mathbf{C}_{\mathbf{l},\mathbf{c}} = \psi \mathbf{M}_{\mathbf{l},\mathbf{c}}, \quad \text{and} \tag{41}$$

$$\mathbf{K}_{\mathbf{l},\mathbf{c}} = \begin{bmatrix} \frac{EA}{L} & 0 & 0 & -\frac{EA}{L} & 0 & 0 \\ 0 & \frac{12EI}{L^3} & \frac{6EI}{L^2} & 0 & -\frac{12EI}{L^3} & \frac{6EI}{L^2} \\ 0 & \frac{6EI}{L^2} & \frac{4EI}{L} & 0 & -\frac{6EI}{L^2} & \frac{2EI}{L} \\ -\frac{EA}{L} & 0 & 0 & \frac{EA}{L} & 0 & 0 \\ 0 & -\frac{12EI}{L^3} & -\frac{6EI}{L^2} & 0 & \frac{12EI}{L^3} & -\frac{6EI}{L^2} \\ 0 & \frac{6EI}{L^2} & \frac{2EI}{L} & 0 & -\frac{6EI}{L^2} & \frac{4EI}{L} \end{bmatrix}, \tag{42}$$

where $\mathbf{l} = \mathbf{c} = \{1, 2, 3, 4, 5, 6\}$ for the superior beam and $\mathbf{l} = \mathbf{c} = \{19, 20, 21, 22, 23, 24\}$ for the inferior beam; $m = \rho_e AL/420$; $L = 2a$, ρ_e and A are, respectively, the length, density and cross-section area of the beam element; E is the Young's modulus of the elastic material and I is the moment of inertia of the beam element cross-section; and $\psi \in \Re$, considering mass proportionality for damping. In spite of damping features present in the elastic aluminum beam (see Table 1), since the damping characteristics of the viscoelastic material is considerably superior to those related to the elastic material, it is adopted $\psi = 0$ for the sandwich model.

4.2. Contribution of the quadrilateral viscoelastic element

The quadrilateral linear viscoelastic plate part of the sandwich element is obtained from a linear plate elastic finite element presented in Fig. 11, whose displacement field is defined in

$$u(x,y) = \frac{1}{4ab}(-q_7 + q_{10} + q_{13} - q_{16})xy + (-q_7 + q_{10} - q_{13} + q_{16})bx + (q_7 + q_{10} - q_{13} - q_{16})ay + \frac{1}{4}(q_{16} + q_7 + q_{10} + q_{13}), \tag{43}$$

$$v(x,y) = \frac{1}{4ab}(q_{11} + q_{14} - q_{17} - q_8)xy + (q_{17} + q_{11} - q_{14} - q_8)bx + (q_{11} + q_8 - q_{17} - q_{14})ay + \frac{1}{4}(q_{17} + q_8 + q_{11} + q_{14}), \tag{44}$$

where $u(x,y)$ and $v(x,y)$ are the horizontal and vertical displacement fields, respectively, q_{10}, q_{11}, q_7, q_8, q_{13}, q_{14}, q_{16} and q_{17} (numbered in Fig. 11) are the nodal displacements; $2a$ and $2b$ are, respectively, the height and width of the element.

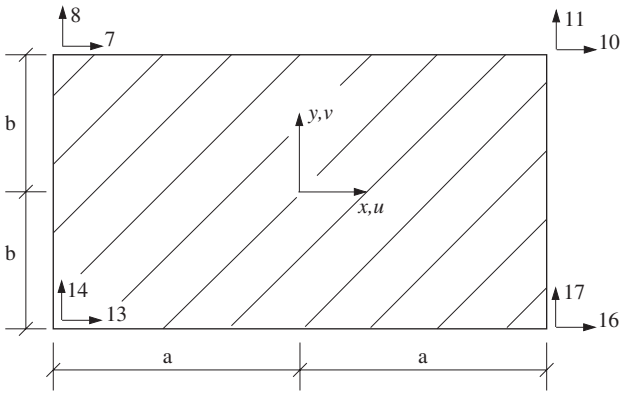

Fig. 11. Quadrilateral linear plate elastic finite element.

For the adopted interpolation functions, the quadrilateral linear plate viscoelastic element contribution for the super element matrix model **K** is presented in the following equations:

$$\mathbf{K}_{\mathbf{l}_1,\mathbf{c}_1} = t(\varepsilon+\alpha)\begin{bmatrix} k_1^e & k_2^e & k_3^e & k_4^e & -\frac{k_1^e}{2} & -k_2^e & k_5^e & -k_4^e \\ k_2^e & k_6^e & -k_4^e & k_7^e & -k_2^e & -\frac{k_6^e}{2} & k_4^e & k_8^e \\ k_3^e & -k_4^e & k_1^e & -k_2^e & k_5^e & k_4^e & -\frac{k_1^e}{2} & k_2^e \\ k_4^e & k_7^e & -k_2^e & k_6^e & -k_4^e & k_8^e & k_2^e & -\frac{k_6^e}{2} \\ -\frac{k_1^e}{2} & -k_2^e & k_5^e & -k_4^e & k_1^e & k_2^e & k_3^e & k_4^e \\ -k_2^e & -\frac{k_6^e}{2} & k_4^e & k_8^e & k_2^e & k_6^e & -k_4^e & k_7^e \\ k_5^e & k_4^e & -\frac{k_1^e}{2} & k_2^e & k_3^e & -k_4^e & k_1^e & -k_2^e \\ -k_4^e & k_8^e & k_2^e & -\frac{k_6^e}{2} & k_4^e & k_7^e & -k_2^e & k_6^e \end{bmatrix}, \tag{45}$$

where $\mathbf{l}_1 = \mathbf{c}_1 = \{10, 11, 7, 8, 13, 14, 16, 17\}$; $k_1^e = r^2 d_1 + d_3/3r$; $k_2^e = d_2 + d_3/4$; $k_3^e = -2r^2 d_1 - d_3/6r$; $k_4^e = d_2 - d_3/4$; $k_5^e = r^2 d_1 - 2d_3/6r$ $k_6^e = r^2 d_3 + d_1/3r$; $k_7^e = -2r^2 d_3 - d_1/6r$; $k_8^e = r^2 d_3 - 2d_1/6r$; $d_1 = 1/1 - v^2$; $d_2 = 1 - v/2(1 - v^2)$; $d_3 = v/1 - v^2$; v is the Poisson ratio of the viscoelastic material; $r = b/a$; $2a$, $2b$ and t are, respectively, the length, height and thickness of the quadrilateral element;

$$\mathbf{K}_{\mathbf{l}_2,\mathbf{c}_2} = \mathrm{diag}\{\alpha, \alpha, \alpha, \alpha, \alpha\}, \tag{46}$$

where $\mathbf{l}_2 = \mathbf{c}_2 = \{25, 26, 27, 28, 29\}$; and

$$\mathbf{K}_{\mathbf{l}_3,\mathbf{c}_3} = \begin{bmatrix} +7.3098\mathrm{e}-1 & -3.7222\mathrm{e}+1 & +0.0000\mathrm{e}+0 & -2.1556\mathrm{e}+1 & +2.8246\mathrm{e}+0 \\ -6.0783\mathrm{e}+1 & +1.7867\mathrm{e}+0 & -3.5108\mathrm{e}+1 & +0.0000\mathrm{e}+0 & +3.3968\mathrm{e}-2 \\ -7.3098\mathrm{e}-1 & -3.7222\mathrm{e}+1 & +0.0000\mathrm{e}+0 & +2.1556\mathrm{e}+1 & -2.8246\mathrm{e}+0 \\ -6.0783\mathrm{e}+1 & -1.7867\mathrm{e}+0 & +3.5108\mathrm{e}+1 & +0.0000\mathrm{e}+0 & +3.3968\mathrm{e}-2 \\ +7.3098\mathrm{e}-1 & +3.7222\mathrm{e}+1 & +0.0000\mathrm{e}+0 & +2.1556\mathrm{e}+1 & +2.8246\mathrm{e}+0 \\ +6.0783\mathrm{e}+1 & +1.7867\mathrm{e}+0 & +3.5108\mathrm{e}+1 & +0.0000\mathrm{e}+0 & -3.3968\mathrm{e}-2 \\ -7.3098\mathrm{e}-1 & +3.7222\mathrm{e}+1 & +0.0000\mathrm{e}+0 & -2.1556\mathrm{e}+1 & -2.8246\mathrm{e}+0 \\ +6.0783\mathrm{e}+1 & -1.7867\mathrm{e}+0 & -3.5108\mathrm{e}+1 & +0.0000\mathrm{e}+0 & -3.3968\mathrm{e}-2 \end{bmatrix}, \tag{47}$$

where $\mathbf{l}_3 = \{10, 11, 7, 8, 13, 14, 16, 17\}$ and $\mathbf{c}_3 = \{25, 26, 27, 28, 29\}$. The eigenvalue problem involved in the solution of the viscoelastic stiffness matrix leads to a complex algebraic solution. For this reason, numerical values resulting from $r = 4.8000\mathrm{e}-02$, thickness $= 24$ mm and Poisson's ratio $= 0.25$ are presented in Eq. (47).

The quadrilateral linear plate viscoelastic element contribution for the super element model matrices **M** and **C** is presented in the following equations, respectively

$$\mathbf{M}_{\mathbf{l},\mathbf{c}} = \mathrm{diag}\left\{\mu, \mu, \mu, \mu, \mu, \mu, \mu, \mu, \frac{\alpha}{\delta}, \frac{\alpha}{\delta}, \frac{\alpha}{\delta}, \frac{\alpha}{\delta}, \frac{\alpha}{\delta}\right\}, \tag{48}$$

$$\mathbf{C}_{\mathbf{l},\mathbf{c}} = \mathrm{diag}\left\{0, 0, 0, 0, 0, 0, 0, 0, \frac{\alpha\beta}{\delta}, \frac{\alpha\beta}{\delta}, \frac{\alpha\beta}{\delta}, \frac{\alpha\beta}{\delta}, \frac{\alpha\beta}{\delta}\right\}, \tag{49}$$

where $\mathbf{l} = \mathbf{c} = \{10, 11, 7, 8, 13, 14, 16, 17, 25, 26, 27, 28, 29\}$, $\mu = \rho_v abt$, being ρ_v the viscoelastic material density.

4.3. Contribution of the four connection elements

The principal features of the implemented connection elements are: they do not increase neither mass nor damping of the super element model and they should assure that the deformed shape of each beam element cross-section remains perpendicular to their respective longitudinal deformed lines. These features assure the introduction of shear deformation in the viscoelastic core model as presented in Fig. 10 and imply null mass and damping matrices whose contributions for the super element stiffness model matrix may be expressed by

$$\mathbf{K}_{\mathbf{l},\mathbf{c}} = \begin{bmatrix} \frac{E_\infty A}{e} & 0 & 0 & -\frac{E_\infty A}{e} & 0 & 0 \\ 0 & \frac{12E_\infty I}{e^3} & \frac{6E_\infty I}{e^2} & 0 & -\frac{12E_\infty I}{e^3} & \frac{6E_\infty I}{e^2} \\ 0 & \frac{6E_\infty I}{e^2} & \frac{4E_\infty I}{e} & 0 & -\frac{6E_\infty I}{e^2} & \frac{2E_\infty I}{e} \\ -\frac{E_\infty A}{e} & 0 & 0 & \frac{E_\infty A}{e} & 0 & 0 \\ 0 & -\frac{12E_\infty I}{e^3} & -\frac{6E_\infty I}{e^2} & 0 & \frac{12E_\infty I}{e^3} & -\frac{6E_\infty I}{e^2} \\ 0 & \frac{6E_\infty I}{e^2} & \frac{2E_\infty I}{e} & 0 & -\frac{6E_\infty I}{e^2} & \frac{4E_\infty I}{e} \end{bmatrix}, \tag{50}$$

where $\mathbf{l} = \mathbf{c} = \{8, 7, 9, 2, 1, 3\}$ for the connection element #1; $\mathbf{l} = \mathbf{c} = \{11, 10, 12, 5, 4, 6\}$ for the connection element #2; $\mathbf{l} = \mathbf{c} = \{20, 19, 21, 14, 13, 15\}$ for the connection element #3; $\mathbf{l} = \mathbf{c} = \{23, 22, 24, 17, 16, 18\}$ for the connection element #4; $E_\infty = 100E$; and $2e$ is the height of the elastic beams.

The sandwich finite element model matrices presented herein consider identical external layers (beam elements). In the cases where the external layers are not identical, matrices **M**, **C** and **K** must be adapted due to differences between the cross-section and the material properties of each beam element.

5. Validation of the proposed finite element model

The first validation test is to verify if the proposed super finite element model is able to simulate the dynamic behavior of a purely elastic beam. To this end the first three natural frequencies of the aluminum made clumped–free elastic beam model presented in Fig. 12 are evaluated through the solution of the classic eigenvalue problem:

$$(\mathbf{K}^s - \omega_n^2 \mathbf{M}^s)\phi_n = \mathbf{0}, \tag{51}$$

where $\mathbf{K}^s$ and $\mathbf{M}^s$ are, respectively, stiffness and mass matrices of the system obtained using the proposed finite element model; s denotes system matrices; ω_n ($n = 1 \ldots 3$) are the circular natural undamped frequencies with the respective mode shapes ϕ_n.

As the core material is modelled as purely elastic, dissipation variables must be eliminated; Young's modulus is considered constant ($E' = \varepsilon$); and loss factor was set to zero ($\alpha = 0$). Other physical properties of the modelled aluminum are: Young's modulus: 68.70 GPa; density: 2690 kg/m^3; and Poisson ratio: 0.33.

Table 3 compares theoretical natural frequencies obtained using Eq. (6) to the ones obtained using the proposed finite element model, showing good agreement. In this analysis 500 super elements were used.

The second validation test is carried out through comparisons between frequency-domain responses obtained using the proposed finite element model and a classic formulation for computational modelling of frequency-dependent properties of viscoelastic materials. The adopted model is obtained by replacing the elastic core of the beam used in the first validation test by the experimentally tested viscoelastic material ($\alpha = 5.26$ MPa, $\beta = 55.59 \times 10^6$ s^{-1}, $\delta = 6.98 \times 10^9$ s^{-2} and $\varepsilon = 0.58$ MPa). Other physical properties of the modelled viscoelastic material are: density: 795 kg/m^3; and Poisson's ratio: 0.25.

The analysis referred as classic frequency-domain analysis of the modelled clumped–free sandwich beam was carried out using the following equation by updating Young's modulus (E^*) for each frequency (ω) and

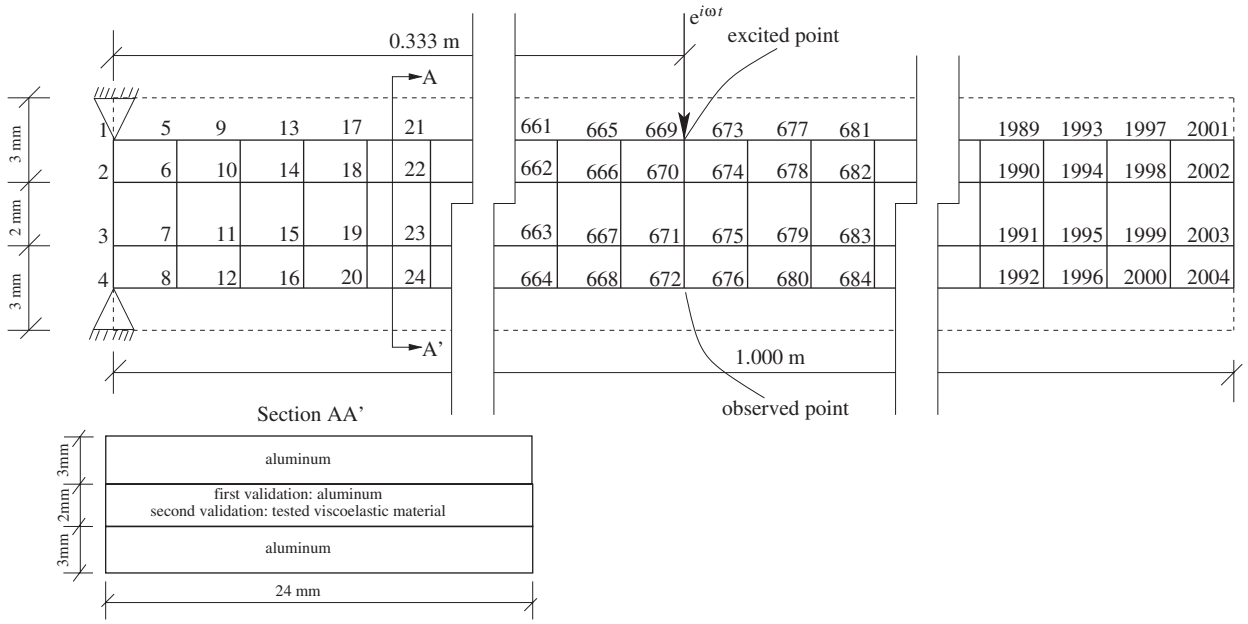

Fig. 12. Finite element model of the validation test.

Table 3
Comparison between theoretical and finite element model natural frequencies of the first validation test

Natural frequencies (Hz)	Theoretical	Finite element model	Percentage difference
f_1	6.53	6.64	1.68
f_2	40.93	41.63	1.71
f_3	114.61	116.51	1.66

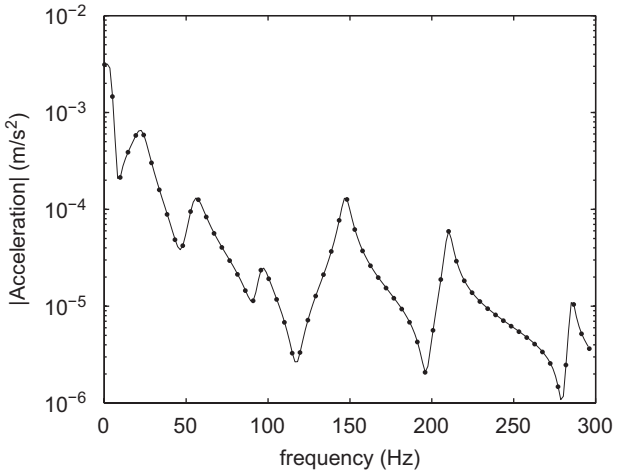

Fig. 13. Comparison between classic and Golla–Hughes method frequency-domain response.

eliminating dissipation variables

$$\mathbf{q}(\omega) = [\mathbf{K}^s(\omega) - \omega^2 \mathbf{M}^s]^{-1} \mathbf{f}(\omega), \tag{52}$$

where $\mathbf{K}^s(\omega)$ is the stiffness matrix of the system, now depending on $E^*(\omega)$ value.

The GHM frequency-domain response may be obtained from the following equation. It is important to notice that the proposed model does not require Young's modulus update although dissipation variables are introduced

$$\begin{Bmatrix} \dot{\mathbf{q}}(\omega) \\ \dot{\mathbf{y}}(\omega) \end{Bmatrix} = [\mathbf{K}^s + \mathrm{i}\omega\mathbf{C}^s - \omega^2\mathbf{M}^s]^{-1} \begin{Bmatrix} \mathbf{f}(\omega) \\ \mathbf{0} \end{Bmatrix}. \tag{53}$$

Fig. 13 compares GHM frequency-domain response with classic analysis counterpart for an excitation vector having one single component applied in the degree-of-freedom presented in Fig. 12. It is clearly noticed that classic and GHM analysis lead to the same result. The same practical values results for the second

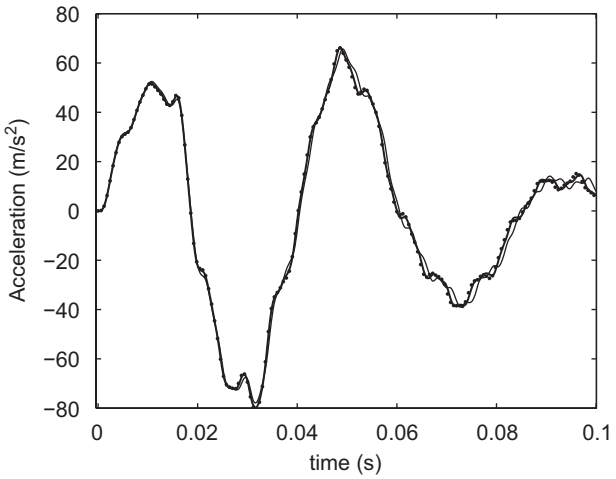

Fig. 14. Convergence analysis of the 1.0 m long beam finite element model: dotted line, thick solid line and fine solid line present results for 48, 24 and 12 super element model, respectively.

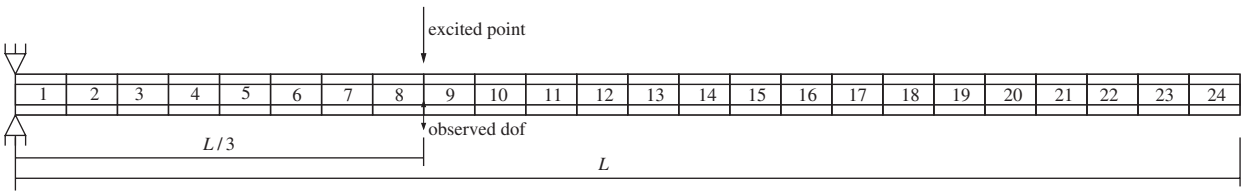

Fig. 15. Adopted finite element model (only the super elements are numbered herein).

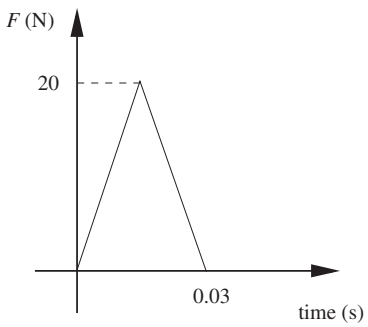

Fig. 16. Excitation function.

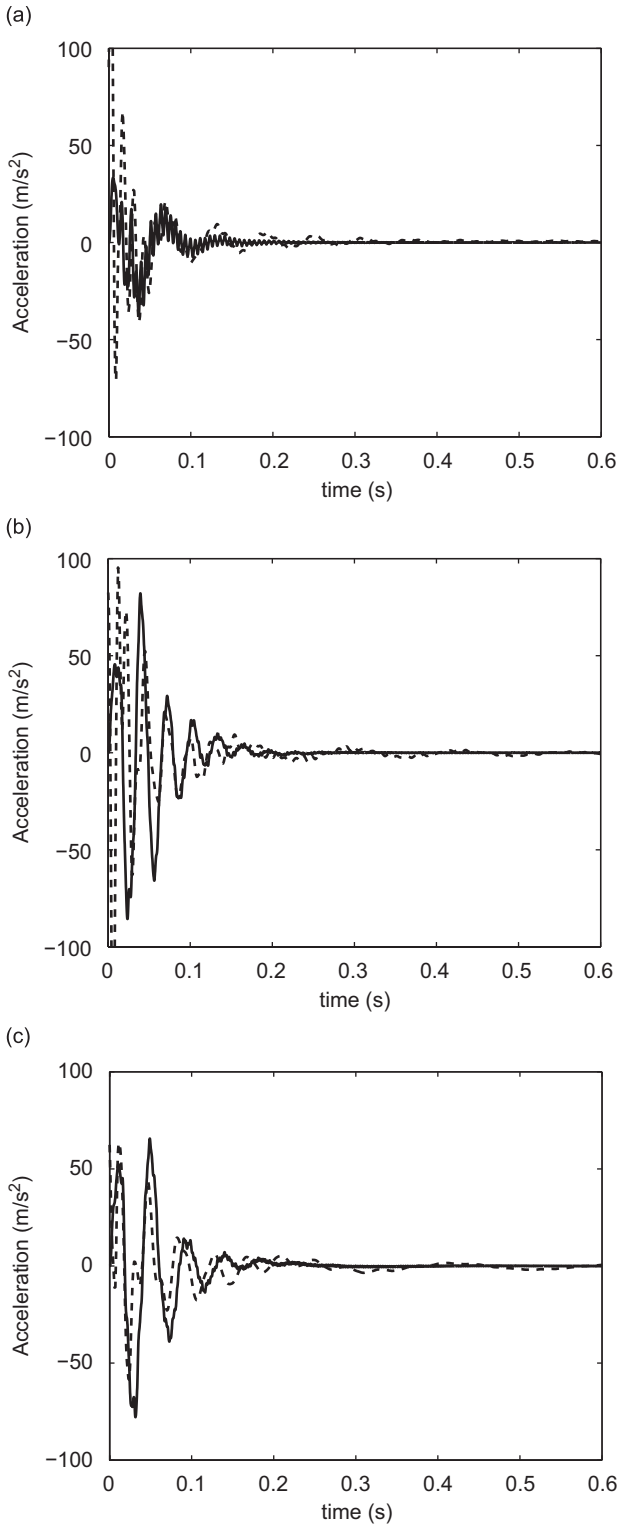

Fig. 17. Comparisons between numerical and experimental counterpart. In these graphics, dashed and solid lines are related to experimental and numerical results, respectively: (a) length:0.5 m; (b) length:0.8 m; (c) length: 1.0 m.

validation test may be achieved by using a finite element model with 24 super elements. Another important point to observe is that time-domain analysis through GHM formulation is very simple since the stiffness matrix is constant.

6. Example of numerical application

The time-domain dynamic behavior of the three sandwich beams experimentally tested in Section 3 were computationally modelled with the sandwich element proposed in this work.

The three finite element models were adopted after a convergence analysis. Results for a free vibration test with impact load applied in models with 12, 24 and 48 sandwich super elements were analyzed and it was verified, by regarding Fig. 14, that results for 24 and 48 are practically coincident. Due to this fact, the adopted models have 24 super elements, as shown in Fig. 15.

The super element finite element matrices may be calculated using equations of Section 4. For the 24 super elements used in the discretization, it implies 332 physical degree-of-freedom and 120 dissipation variables. Physical and geometric properties adopted for the models are the same used in validation tests.

As the hammer excitation impact was not measured, the three adopted sandwich beam models were submitted to the excitation bilinear function model presented in Fig. 16. The maximal amplitude of this excitation function (20 N) was evaluated by multiplying the hammer mass (0.20 g) by the mean acceleration level of the beams (approximately $100\,m/s^2$) at impact instant extracted from Fig. 6, since hammer and beam mass are similar. The time of load application (0.03 s) was evaluated as approximately 15% of the first natural period of the simple set. The adopted impact duration time is close to the one measured in Ref. [29].

The set of 452 differential equations was integrated using Newmark method with 8333 time steps of 0.00012 s, consuming 95% of the total CPU processing time which reached 7.05 s in a Matlab© implementation on a Pentium© IV 2.8 GHz. The time-domain responses were filtered with a low-pass filter in 200 Hz, as it was made in the experimental tests.

Figs. 17(a)–(c) show comparisons between experimental and numerical time responses for the three tested cases, indicating a reasonable correlation, specially for the 1.0 and 0.8 length beams. The differences between numerical and experimental results are probably due to uncertainties in the experimental program and in the adopted impact model. In a qualitative point of view, these results are almost equivalent, considering that the acceleration level in the time interval 0–0.1 s is practically the same and also that the acceleration level past 0.3 s is practically negligible for both analysis. These results demonstrate the good performance of the proposed finite element model in a time-domain simulation of a sandwich viscoelastic beam dynamic behavior.

Table 4 presents experimental and numerical results obtained for the first three natural frequencies of the three sandwich beams, showing that the differences between these results are inferior to 14.50%. Such

Table 4
Comparisons between experimental and numerical results for the sandwich set

	$L = 1.00\,m$	$L = 0.80\,m$	$L = 0.50\,m$
f_1^{exp}	5.05	7.55	16.95
f_1^{num}	4.32	6.61	14.86
$(f_1^{num} - f_1^{exp})/f_1^{exp}$	−14.46%	−12.45%	−12.33%
f_2^{exp}	24.54	37.13	79.33
f_2^{num}	22.88	32.05	88.75
$(f_2^{num} - f_2^{exp})/f_2^{exp}$	−6.76%	−13.68%	11.87%
f_3^{exp}	60.13	93.18	184.44
f_3^{num}	53.66	83.16	166.83
$(f_3^{num} - f_3^{exp})/f_3^{exp}$	−10.76%	−10.75%	−9.55%

(^{exp}) denotes mean experimental values; (^{num}) denotes numerical values; and ($_n$) denotes the nth natural frequency. Frequencies are presented in Hz.

differences may be explained by the quality of the curve fitting obtained from the four parameters GHM model presented herein (see Figs. 7 and 8).

7. Conclusions

A GHM-based sandwich finite element model was presented in this work. All the element matrices were developed and presented as well as all experimental procedures necessary to evaluate GHM parameters. A validation test was carried out by comparing frequency-domain response of the proposed finite element model to the ones obtained by theoretical and classic formulations. A numerical model using the proposed finite element model was dynamically tested and the obtained results were compared with experimental results counterpart, showing good agreement.

Acknowledgments

The authors wish to thank the CNPq—Conselho Nacional de Desenvolvimento Científico e Tecnológico; FAPEMIG—Fundação de Amparo à Pesquisa do Estado de Minas Gerais; and UFJF—Universidade Federal de Juiz de Fora for the financial support. The authors also thank B.Sc. students: Eduardo Castro and Emanuel Uieira.

References

[1] J.G.J. Beijer, J.L. Spoormaker, Solution strategies for FEM analysis with nonlinear viscoelastic polymers, *Computers & Structures* 80 (2002) 1213–1229.
[2] A.D. Mesquita, H.B. Coda, New methodology for the treatment of two dimensional viscoelastic coupling problems, *Computer Methods in Applied Mechanics and Engineering* 192 (2003) 1911–1927.
[3] H. Oberst, K. Frankenfeld, Damping of the bending vibrations of thin laminated metal beams connected through adherent layer, *Acustica* 2 (1952) 181–194 (in German).
[4] E.M. Kervin Jr., Damping of flexural waves by a constrained viscoelastic layer, *Journal of the Acoustical Society of America* 31 (1959) 952–962.
[5] D. Ross, E.E. Ungar, E.M. Kervin Jr., Damping of plate flexural vibrations by means of viscoelastic laminate, *ASME, Structural Damping Section* 3 (1959) 49–88.
[6] F.S. Barbosa, Computational Modeling of Structures with Damper Viscoelastic Layers PhD Thesis, COPPE/UFRJ—Federal University of Rio de Janeiro, Brazil, 2000 (in Portuguese).
[7] F.S. Barbosa, R.C. Battista, A time and frequency-domain modeling of structures with damper viscoelastic layers, *Proceedings of the of the XXIX Jornadas Sudamericanas de Ingeniería Estructural, 29th South American Structural Engineering Conference*, November, Punta del Este, Uruguay, 2000 (CDROM) (in Portuguese).
[8] R.C. Battista, E.M. Batista, M.S. Pfeil, Experimental tests on a prototype scale model of the slender sandwich concrete-viscoelastic-steel deck for rehabilitation of the Rio–Niterói bridge, Rio de Janeiro, Brazil. Contract Report COPPETEC ET-150771 with Ponte S.A.—Concessionaire of the Rio–Niterói Bridge, 1998 (in Portuguese).
[9] R.C. Battista, M.S. Pfeil, Strengthening fatigue cracked orthotropic decks with composite layers, *Proceedings of International Association for Bridge and Structural Engineering—IABSE Symposium*, August 1999, Vol. II, Rio de Janeiro, Brazil, 1999, pp. 853–860.
[10] P. Mahmoodi, Structural dampers, *ASCE Journal of Structural Division* 95 (8) (1969) 1661–1672.
[11] B. Samali, K.C.S. Kwok, Use of viscoelastic dampers in reducing wind-and earthquake-induced motion of building structures, *Engineering Structure* 17 (9) (1995) 639–654.
[12] R.W. Clough, J. Penzien, *Dynamics of Structures*, third ed., Computers & Structures, Inc., USA, 1995.
[13] C. Qian, Z. Demao, Vibrational analysis theory and application to elastic-viscoelastic composite structure, *Computers & Structures* 37 (4) (1990) 585–595.
[14] M. Kaliske, H. Rothert, Formulation and implementation of three-dimensional viscoelasticity at small and finite strains, *Computational Mechanics* 19 (1997) 228–239.
[15] T.T. Babert, R.A. Maddox, C.E. Orozco, A finite element model for harmonically excited viscoelastic sandwich beams, *Computers & Structures* 66 (1997) 105–113.
[16] J.A. Zapfe, G.A. Lesieure, A discrete layer beam finite element for the dynamic analysis of composite sandwich beams with integral damping layers, *Computers & Structures* 70 (1999) 647–666.
[17] S. Yi, F.L. Shih, M. Ying, Finite element analysis of composite structures with smart constrained layer damping, *Advances in Engineering Software* 29 (3–6) (1990) 265–271.

[18] D.F. Golla, P.C. Hughes, Dynamics of viscoelastic structures—a time-domain, finite element formulation, *Journal of Applied Mechanics* 52 (1985) 897–906.
[19] M.A. Biot, Variational principles in irreversible thermodynamics with application to viscoelasticity, *Physical Review* 97 (6) (1955) 1463–1469.
[20] R.L. Bagley, P.J. Torvik, A theoretical basis for the application of fractional calculus to viscoelasticity, *Journal of Rheology* 27 (1983) 210.
[21] K.E. Barrett, A.C. Gotts, Finite element analysis of a compressible dynamic viscoelastic sphere using FFT, *Computers & Structures* 80 (2002) 1615–1625.
[22] American Society for Testing and Materials, ASTM E 756-04e1, Standard Test Method for Measuring Vibration-Damping Properties of Materials, Book of Standards, Vol. 04.06—Thermal Insulation, Environmental Acoustics 2004.
[23] Kyowa Electronic Instruments Co. Ltd. *Accelerometers User Guide*, 2007. ⟨http://www.kyowa-ei.co.jp/english/index_e.htm⟩.
[24] Lynx Tecnologia Eletrónica, *ADS2000 User Guide 2007*, ⟨http://www.lynxtec.com.br/⟩.
[25] J.C. Asmussen, Modal Analysis Based on the Random Decrement Technique—Application to Civil Engineering Structures, Ph.D. Thesis, Aalborg University, Denmark, 1998.
[26] D.J. Ewins, *Modal Testing: Theory, Practice and Application*, Research Studies Press, England, 2000.
[27] C. Cremona, F.S. Barbosa, A. Alvandi, Modal identification under ambient excitation: application to bridge monitoring, *Mécanique & Industries* 4 (2003) 259–271.
[28] R.G. Faisca, Characterization of Viscoelastic Materials as Structural Dampers, MSc Thesis, COPPE/UFRJ—Federal University of Rio de Janeiro, Brazil, 1998 (in Portuguese).
[29] S. Vanlanduit, F. Daerden, P. Guillaume, Experimental modal testing using pressurized air excitation, *Journal of Sound and Vibration* 299 (2007) 8398.